Int. J. Heat Mass Transfer. Vol. 24, No. 9, pp. 1503–1511, 1981.
Printed in Great Britain

0017-9310/81/091503-09 $02.00/0

MEASUREMENTS OF FLUID AND THERMAL TRANSPORT IN VERTICAL BUOYANCY INDUCED FLOWS IN COLD WATER

Z. H. QURESHI

Department of Energy Engineering, College of Engineering,
University of Illinois at Chicago Circle, Chicago, IL 60680, U.S.A.

and

B. GEBHART

University of Pennsylvania, Philadelphia, PA 19104, U.S.A.

(*Received* 17 *September* 1980 *and in revised form* 9 *March* 1981)

Abstract — Measurements of transport quantities are obtained in a vertical buoyancy induced flow along a uniform flux surface (1.3 m high) in water at 4°C. Velocity and temperature fields are determined at various downstream locations for several values of flux level ranging from 368 to 3617 W/m^2. Both average and disturbance quantities are measured and compared with theory. A simultaneous velocity and thermal transition is found. Due to a nonlinear density dependence on temperature the transition is delayed. A new parameter is suggested which predicts the beginning of transition. The frequency filtering in the laminar and early transition region was found not to be very sharp, as also predicted by the calculations. The predicted filtered frequency, $B^* = 1.343$ is confirmed by the experimental data obtained.

NOMENCLATURE

- B^*, characteristic frequency for a uniform flux surface condition;
- E, anemometer output [V];
- E_0, anemometer output at zero velocity [V];
- f, physical frequency;
- f', dimensionless velocity;
- g, gravitational force [m/s^2];
- Gr_x^*, modified local Grashof number;
- k, thermal conductivity [W/m °C];
- Nu_x, local Nusselt number;
- P, pressure [bars];
- Pr, Prandtl number;
- q, $= q(s, p)$, exponent in the density equation;
- q'' surface heat flux [W/m^2];
- Ra_x^*, modified local Rayleigh number;
- s, salinity [ppt];
- $s(\eta)$, disturbance temperature amplitude function;
- t, temperature [°C];
- U, average velocity in x-direction [m/s];
- u, v, disturbance velocity components [m/s];
- x, y, z, coordinates.

Greek symbols

- α, $= \alpha(s, p)$, temperature coefficient [1/°C^q];
- ν, kinematic viscosity [m^2/s];
- ρ, $= \rho(t, s, \rho)$, density of water [kg/m^3];
- ϕ, generalized temperature;
- η, similarity variable.

Subscripts

- f, local fluid temperature;
- m, extremum condition;
- 0, at the fluid–solid interface;
- r, reference;
- ∞, unstratified quiescent ambient medium.

INTRODUCTION

BUOYANCY-induced flows are widely encountered in nature and industry. The driving force in such flows is the density gradients present in an ambient medium in a gravitational field. These gradients may arise due to thermal, salinity and pressure gradients in the ambient medium. Depending upon the nature of the circumstances, any one or more of the above may cause the motion. In general the buoyancy forces due to these gradients may be in the same direction or oppose each other. To analyze such flows, a precise dependence of density upon temperature, salinity and pressure level must be known. The density extremum in pure water at atmospheric pressure, at about 3.98°C is well known. An extremum also occurs in saline water, up to a salinity level of about 25.5 parts per thousand (ppt). It also occurs at elevated pressures, up to about 300 bars in pure water; in local thermodynamic equilibrium. An extremum is found well beyond these conditions in non-equilibrium circumstances. In buoyancy induced flow driven by differing temperatures around the extremum condition, maximum density conditions may arise to influence the motion. In fact, given the dependence of density on temperature, salinity and pressure and the dependence of extremum temperature on both salinity and pressure, several density extrema may conceivably occur across a given flow region.

Generally the buoyancy force $g(\rho_r - \rho)$ is expressed linearly in terms of differences $(t - t_r)$ and $(s - s_r)$, using the respective volumetric coefficients of expansion as appropriate constants. This is usually not a reasonable formulation when a density extremum condition arises. Gebhart and Mollendorf [1] developed a simple yet very accurate density relationship for water around the density extremum condition for salinity levels up to 35 ppt and 1000 bars pressure. Using this relation they were able [2] to find similarity solutions for two-dimensional boundary layer flow induced by the combined buoyancy effects of thermal and saline diffusion.

This study considers a vertical surface 1.3 m high which dissipates uniform heat flux in water at 4°C. For such a surface condition similarity results only when the ambient medium is at a temperature condition at which density extrema occurs. The previous studies of free convection along vertical surfaces in cold water include both analytical treatment and experimental results. The first detailed heat transfer measurements in water, under conditions of density inversion were apparently made by Ede [3] on a 10.2 cm high electrically heated plate. This was, at least approximately, the uniform flux surface condition. The plate data were obtained for three conditions: (a) t_0 and $t_\infty < 4$°C; (b) $t_0 > 4$°C $> t_\infty$; and (c) t_0 and $t_\infty > 4$°C. Specific results were compared with Merk's [4] predictions. Both bad and good agreement was shown. There is considerable doubt that such weak and complicated flows, over small surfaces, are appropriately modelled as Merk has, with an integral boundary layer treatment.

Schechter and Isbin [5], using the buoyancy force approximations developed by Merk and an integral method analysis with analog solution, considered a vertical surface in water around 4°C. In some experiments they found dual motion (up and down) and conceded the preclusion of a unified theory of such processes. The analysis of Gebhart and Mollendorf [2] suggests that choosing conventional profiles is quite unrealistic for some such flows.

A theoretical analysis for a semi-infinite isothermal vertical plate in water at 4°C was considered by Goren [6]. The buoyancy $\Delta\rho$ was taken as $\rho_m \alpha (t - t_m)^2$, where $\alpha = 8.0 \times 10^{-6}$ $(°C)^{-2}$. No additional parameters arise, and an analog computer solution was given for $Pr = 11.4$. It was shown that for water at 4°C the convective velocities were reduced by about 8 and 80-fold from those in water at 20°C for temperature variations of 1°C and 10^{-2}°C, respectively. The accuracy of the analysis was restricted to the temperature range of 0–8°C. Vanier and Tien [7] extended the study of Goren [6] by approximating the buoyancy $\Delta\rho$ by a sum of linear, square and cubic terms in $(t - t_m)$, according to the density data of Perry [8], as had Merk. The penalty was two t_0 dependent parameters in two new terms in the differential equations. However, the results were applicable for plate temperatures of up to 35°C, but still limited to $t_\infty = t_m$.

Vanier and Tien [9] gave an intensive discussion of the directional tendencies of flow adjacent to a vertical surface in cold water. An analysis used again the density formulation used by Merk [4]. Additional parameters again arise which depend upon three β_i constants of the density formulation and also on t_0 and t_∞. Numerical results were compared with the predictions of Schechter and Isbin [5]. Considerable differences are found. Roy [10] resolved Goren's problem and obtained results about 15% different, as found by Vanier and Tien [9] also.

Using the density equation of [1], a similarity analysis was given by Qureshi and Gebhart [11] for a vertical uniform flux surface in water at $t_\infty = t_m$. The buoyancy force $\Delta\rho$ was taken as

$$\rho_m \alpha(s, p)[t - t_m]^{q(s,p)}.$$

One additional parameter arose in the analysis, $q(s, p)$, which depends upon the ambient salinity and pressure levels. For pure water at atmospheric pressure $q = 1.8948$. The lowest value of $q = 1.5829$ corresponds to an extreme pressure condition of 1000 bars and zero salinity. In the analysis the temperature excess $(t - t_\infty)$ was normalized by the surface temperature excess $(t_0 - t_\infty)$ which is not known *a priori* for a uniform flux surface. In a recent paper, Qureshi and Gebhart [12] have presented a similar boundary layer analysis defining a temperature function d(x), based on surface heat flux for normalization. The resulting flux Grashof number

$$Gr_x^* = \frac{g\alpha(s, p)x^3}{\nu^2}\left(\frac{q''x}{k}\right)^q.$$

For five values of $q(s, p)$ numerical results were obtained over a range of Prandtl number of 8.0–13.0. Following heat transfer correlation in the laminar regime was suggested based on the numerical calculations

$$Nu_x = 0.577(Gr_x^* Pr)^{1/(4+q)}. \tag{1}$$

This correlation is very accurate in the range $q = 1.813$–1.8948. This range corresponds to salinity and pressure levels at which the density extrema occurs under thermodynamic equilibrium. The above relationship can also be used for non-equilibrium circumstances ($q = 1.5829$–1.813) with an inaccuracy of less than 1%.

Nondimensional velocity and temperature profiles across the boundary region were also determined. The measured velocity and temperature data of this study are compared with these profiles.

To the best of our knowledge no previous study on transition of such a flow has been made. Many past studies on transition of a buoyancy induced flow in a medium where the Boussinesq approximation is admissable were summarized by Qureshi and Gebhart [13]. For the temperature conditions far from t_m, where density may be taken as a linear function of temperature differences, different transition criteria were discussed.

With an ambient at a temperature at which density extrema occurs, the resulting flow is less vigorous. This results in low thermal transports rates. The transition to turbulence is delayed. Both fluid mechanic and thermal transition were measured using hot film anemometer and thermocouple probes in the boundary region.

APPARATUS

The experimental apparatus used in this study is essentially the same as described in [13]. A vertical surface 130.5 cm long, 46.6 cm wide and 0.038 cm thick is electrically heated in a very well-insulated water tank of dimensions $1.83 \times 0.662 \times 1.83$ m high. The surface consists of two 0.00127 cm thick Inconel 600 foils separated by layers of Teflon. A uniform foil thickness assured the uniform flux surface condition. Twenty-four, 0.0127 cm copper–constantan thermocouples were placed along the vertical center line (in the middle of the Teflon layers) of the surface. The water was filtered, de-aerated under 63 cm Hg vacuum and purified to a resistivity level of 1.0 MΩ cm. The high purity level of water is very important because of electrical heating and for the operation of the hot film probe. Fine particles can contaminate the probe and cause its drift.

An important aspect of the experiment was to maintain the ambient temperature level at 4°C. A chiller was used to maintain a low temperature of an ethylene glycol bath containing a stainless steel coil through which the tank water was circulated by the help of a magnetic pump. The stirred tank water was cooled to approximately 3.5°C before the circulation was terminated. An electric heater was then used to heat the water slightly to the desired temperature of 4°C. Tank temperature was monitored at five different locations along a vertical line, to detect any stratification. The tank was well insulated from all the sides and the top. The temperature rise due to heat leakage was very small, less than 0.1°C over the period of 2–3 h. Due to the heat generated by the surface during each experiment, a warm layer collected at the top. This restricted the actual experiment time to 30 min–1 h, depending upon the heating rate.

The surface temperature at different locations downstream from the leading edge was measured by the corresponding thermocouple embedded in the plate assembly. Thermocouple locations are shown in Fig. 1.

Boundary layer temperature and velocity measurements were made by 0.025 mm dia chromel–alumel thermocouple and a Disa hot film probe type 55R14. Data for both the average values and the disturbance levels was recorded on a Beckman R-511 Dynograph. Both probes were mounted on a traversing mechanism capable of moving in all three directions. The closest approach of the probes to the surface was 0.5 mm. Five different downstream, or x locations, were selected for the boundary region traverses. For each location the surface flux was varied in steps from 368 to 3617 W/m^2.

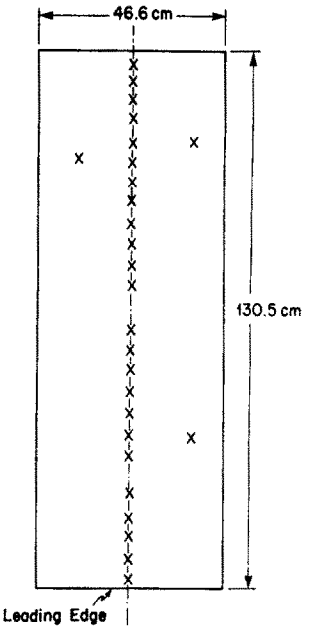

FIG. 1. Thermocouples locations in the plate assembly.

All the experiments were performed during the night to avoid disturbances caused by daytime activity.

HOT FILM CALIBRATION

For velocity measurements in the boundary layer a constant temperature anemometer (Disa type 55D01) with a fiber film probe (55R14) was used. In such probes a nickel film is deposited on a 70 μm dia. quartz fiber. The overall length is 3 mm and sensitive film length is 1.25 mm. The film is protected by a 2 μm quartz coating.

The calibration apparatus used is described in detail in [14]. The probe is moved vertically in a stationary tank by a Disa traversing mechanism (55H01). A variable speed motor is attached to the traversing mechanism. The velocity range obtained is approximately from 0.0083 to 83 cm/s. The velocities encountered in such natural convection flows are very low and fall within this range. The apparatus can move the probe at any angle between vertical and horizontal, at 15° intervals. For this study the probe was moved only in vertical direction. The velocity of the probe is inferred from the time recorded to traverse the probe over a known distance. The anemometer output is recorded on an integrating voltmeter.

In buoyancy induced flows the velocity field is coupled with temperature gradients. For a fixed probe temperature, the output of the anemometer E varies with the velocity levels and the ambient temperature level. To interpret the experimental results it is necessary to uncouple these two effects. For a given velocity level the output decreases with increasing ambient temperature while at a given ambient temperature level the output E increases with increasing velocities. As a probe moves into the thermal boundary layer both temperature and velocity levels in-

crease and their effects on the output are to oppose each other. As the velocity maxima is crossed both factors reduce the output near the surface. Compensation of temperature variation can be accomplished by various methods. See [14] for a discussion of these methods. Hollasch and Gebhart [15] proposed that the heat transfer from the sensor depends primarily on the temperature difference between the sensor and its surroundings. Therefore, the probe may be calibrated at different sensor temperatures in the same ambient temperature. Various calibration curves ($E - E_0$ vs U) correspond to different temperature differences between sensor and the ambient. During the experiment the probe sensor is operated at a constant temperature. By a simultaneous temperature measurement in the boundary layer, the temperature differences between the sensor and the surrounding fluid is known and the appropriate calibration curve may be used. The same method was used by Shaukatullah and Gebhart [16] for the temperature compensation. The anemometer output voltage, above that at zero velocity ($E - E_0$) was plotted against velocity. This method of expressing the calibration was convenient because E_0 could be suppressed on the chart recorder and the signal ($E - E_0$), could be amplified for better resolution. At any particular location in the boundary layer ($E - E_0$) and the fluid temperature was recorded. By third-order Lagrangian interpolation polynomials, the velocity was calculated.

Note that in the above method, the value of E_0 at t_∞ was suppressed on the chart recorder. In fact E_0 decreases as the probe moves toward the surface due to increasing fluid temperature. Very near the surface the output of the anemometer drops below the E_0 value at t_∞. Actually the local value of ($E - E_0$) is still positive. The effect of E_0 drift is prominent. This was ignored in [14]. This is perhaps the reason for the low measured velocities in [14] near the velocity peak.

Another shortcoming of the above method [15] for this study is the assumption that heat transfer from the sensor depends primarily on the temperature difference between the sensor and the fluid. This assumption is reasonable where the fluid properties do not change significantly with the temperatures encountered, particularly when the density is approximately a linear function of temperature. The present experimental study involves temperatures near the density extremum where the buoyancy force depends upon the temperature levels as well. For the above reasons the probe was calibrated at a fixed sensor temperature while the ambient temperature was varied over a range expected in the experiment. A chiller was used to maintain the desired low temperature in the calibration tank. Stratification was dissipated by a stirrer.

It was decided to operate the probe at a constant temperature of 28°C during the actual experiment and the calibration. A set of five calibration curves ($E - E_0$ vs U) were obtained at 4, 8, 12, 16 and 20°C ambient temperatures. Figure 2 shows the variation of zero velocity voltage E_0 with the ambient medium temperature. Following third-order polynomial was used to represent this variation

$$E_0 = 4.376042 + 0.014167t_f - 0.006719t_f^2 + 0.000091t_f^3 \quad (2)$$

where $4°C < t_f < 20°C$.

Five calibration curves are shown in Fig. 3 corresponding to different ambient temperatures. Eighth-order polynomials in the form $U = f(E - E_0)$ gave the best fit to the data points. During the experiment simultaneous measurements of velocity and temperature were taken. Starting from outside the boundary region ($t_\infty = 4°C$) the output of the hot film was measured by a digital voltmeter and this signal was used as a reference line on the chart recorder. The probe was moved towards the plate and data was obtained at approximately 18 locations. At all these locations the value of E_0 was calculated from equation (2) using the local temperature as t_f. For a known value of $E - E_0$ and temperature, the velocity was

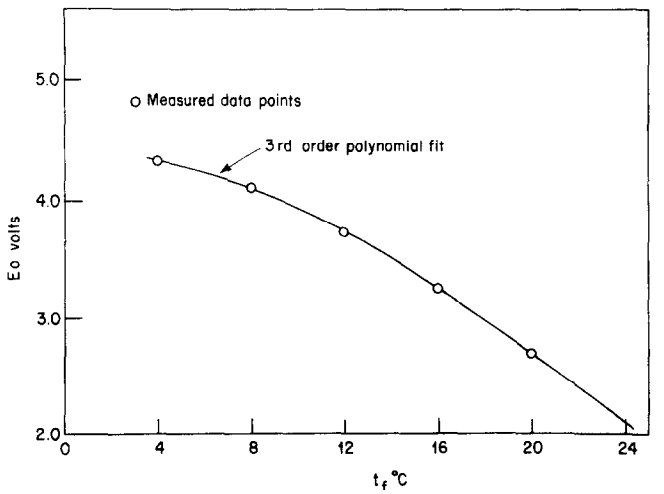

FIG. 2. Zero velocity output voltage E_0 as a function of ambient temperature t_f. Probe sensor temperature 28°C.

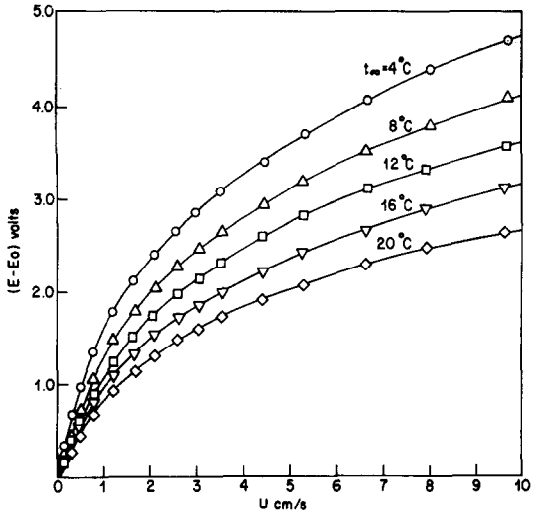

FIG. 3. Anemometer output voltage with respect to 0 velocity voltage ($E - E_0$) as function of velocity U for various ambient temperature levels. Probe temperature 28°C.

calculated from the calibration curves using fourth order Lagrangian interpolation polynomials.

EXPERIMENTAL RESULTS

Experimental results were obtained by traversing the velocity and temperature probes at five different x locations, 32.8, 53.3, 78.6, 89.9, and 124.1 cm from the leading edge. For traverses at each location the surface was loaded with four flux levels, 368, 634, 1389 and 2414 W/m^2 At x = 78.6 cm, a higher value, q'' = 3617 W/m^2, was also used. This amounts to a total of 21 experimental runs. The surface temperature was simultaneously recorded by the thermocouples embedded in the surface. During all the experiments the ambient medium was maintained at 4°C. The results are summarized in two parts. The first part gives the transport data and velocity and temperature fields in the laminar and transition regions. Some data was obtained in the turbulent region also. The transition and disturbance data are presented in the second part.

LOCAL HEAT TRANSFER MEASUREMENTS, VELOCITY AND TEMPERATURE FIELDS

For five flux levels, surface temperature t_0 was measured at 24 downstream locations. Figure 4 shows the $(t_0 - t_\infty)$ variation with downstream distance x in the laminar, transition and turbulence regions. In the laminar region the surface temperature excess is seen to vary as $x^{1/(4+q)}$ as predicted by theory [12] and shown by the solid lines. Using the Boussinesq approximation, $(t_0 - t_\infty)$ varies as $x^{1/5}$. The dashed line represents this later variation. Considerable error due to this approximation in cold water is apparent.

Equation (1) gives the heat transfer correlation in the laminar region proposed by [12] based on calculations. Figure 5 shows all of the experimental local heat transfer data, compared with this correlation. An excellent agreement is obtained up to $Ra_x^* = 10^{14}$, where $Ra_x^* = Gr_x^* Pr$. The following correlation gives the best fit to the data beyond this, in the turbulent region

$$Nu_x = 0.438[Ra_x^*]^{0.19} \quad \text{for} \quad Ra_x^* > 4 \times 10^{15} \quad (3)$$

where

$$Ra_x^* = \frac{q\alpha(s,p)x^3}{\nu^2}\left(\frac{q''x}{K}\right)^{q(s,p)} Pr.$$

All the properties calculated at the film temperature $(t_0 + t_\infty)/2$.

More data is required to check the broader validity of the above correlation. In cold water, a very high value of q'' is required to obtain turbulence over a reasonable length of the plate.

The velocity measurements in the laminar region of the boundary layer are shown in Fig. 6. The hot film data was compensated for the thermal gradients as described above concerning calibration. Calculated

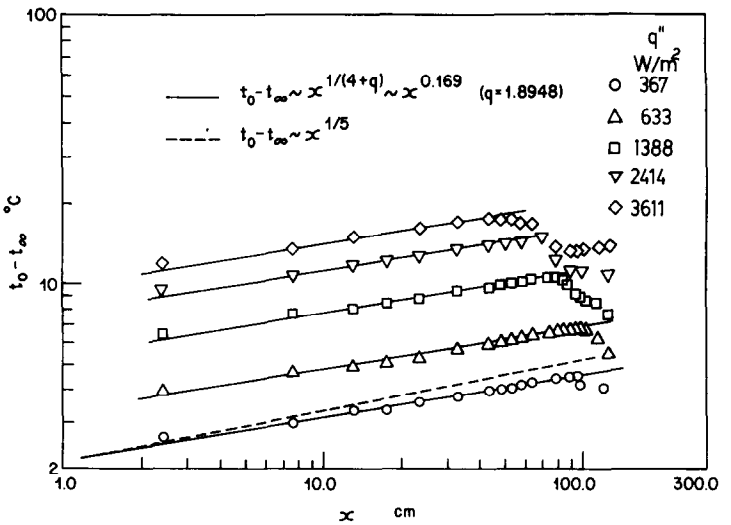

FIG. 4. Surface temperature excess as a function of downstream distance for different surface flux levels.

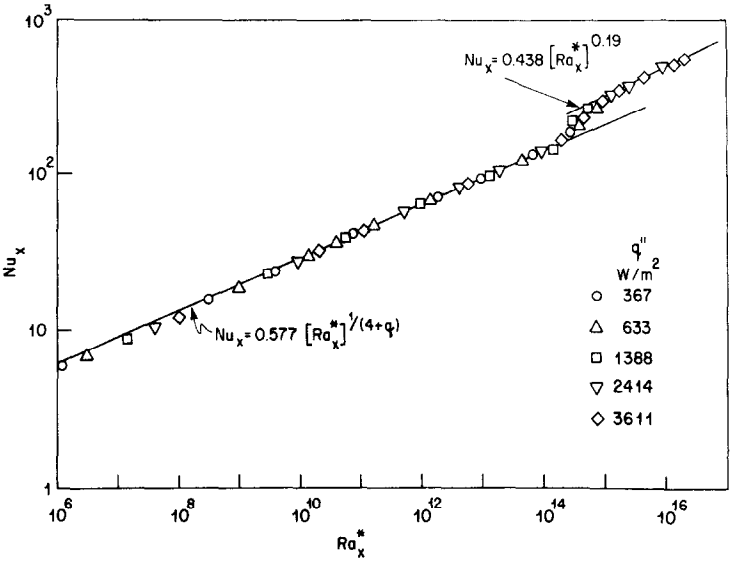

FIG. 5. Nusselt number as a function of modified Rayleigh number in laminar, transition and turbulent region.

profiles (f' vs η) from [12] for various Prandtl numbers are also shown. The data has a good agreement near the surface and the velocity maximum. In the outer part of the boundary layer ($\eta > 2.5$) the data systematically deviates from the calculated profiles. Low velocity levels are measured in this region. In fact, away from the surface the ratio v/u increases. In this region the sensor sees the net flow coming in at a certain angle from vertical. Far out the flow direction is near horizontal. Then the anemometer output E may drop below the zero velocity voltage E_0, depending upon the velocity level. Shaukatullah and Gebhart [17] have discussed this effect in detail. They further showed that there was no appreciable difference between calibrations in vertical flow and in flows included at 30° from vertical. Low measured anemometer output in the outer part of the boundary layer, as seen in Fig. 6, may be attributed to the effect of larger flow direction deviations.

Figure 7 compares the measured and calculated temperature fields. All values are normalized by the surface temperature excess $\phi(0)$. The ordinate then represents $(t - t_\infty)/(t_0 - t_\infty)$, while the abcissa is the similarity variable, η. Data in the laminar region show an excellent comparison. As transition begins the slope near the surface becomes steeper and the boundary layer thickens. Note that in these coordinates (based on laminar analysis) the turbulent profiles cannot be correlated. Due to insufficient turbulent data, no effort is made to correlate the velocity and temperature fields in turbulence.

TRANSITION AND DISTURBANCE FIELD

Beyond a certain downstream location x, depending upon the surface flux level, the laminar flow undergoes the process of transition. The disturbance data of this study shows a simultaneous velocity and thermal transition. Previous studies in water at room tempera-

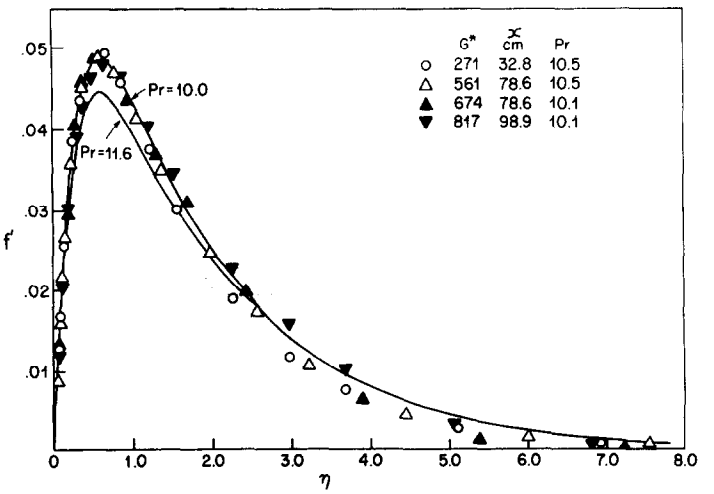

FIG. 6. Mean velocity distribution across the boundary layer.

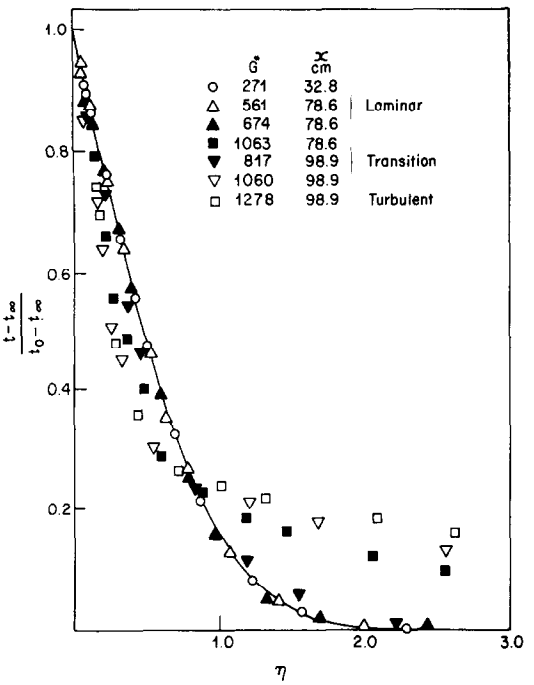

FIG. 7. Mean temperature distribution across the boundary layer.

ture (see [13] for a review of the past studies) and in gases [18] indicated an early fluid-mechanic transition and a subsequent thermal one. Different criteria were used to define and determine transition and different parameters were suggested to correlate the events of transition. Godaux and Gebhart [19] suggested, for a uniform flux surface in water at room temperature, that thermal transition from naturally occurring disturbances began at an approximately constant value of $(q''x)^{1/5} \propto (Gr_x^*)^{1/5}/x^{3/5}$ where $Gr_x^* = g\beta q'' x^4/kv^2$. In the subsequent detailed investigation of a similar flow by Jaluria and Gebhart [20], velocity transition was found to precede thermal transition. The two events were found to begin at different particular values of $G_{BT}^*/x^{2/5}$ where $G^* = 5(Gr_x^*/5)^{1/5}$. Here G_{BT}^* is the value of G^* at the beginning of transition. In dimensional form this parameter represents $(q''x^2)^{1/5}$. The suggested parameter was $G^*(v^2/gx^3)^{2/15}$. A similar type of transition parameter Q_{BT} was proposed by Mahajan and Gebhart [18] for gases to high pressure levels. Dimensionally Q_{BT} represents $G_{BT}^*/x^{2/5}$ and the pressure dependence. In our cold water measurements the functional form of the parameter was found to be different. Both velocity and thermal transition were found to occur for a constant value of $G_{BT}^* x^{1/5}$. Note that G^* for this study is defined as

$$G^* = (4+q)[Gr_x^*/(4+q)]^{1/(4+q)}$$

where

$$Gr_x^* = \frac{qx^3}{v^2}\alpha(s,p)\left(\frac{q''x}{k}\right)^q. \qquad (4)$$

Note that G^* is proportional to $[(q'')^q x^{(3+q)}]^{1/(4+q)}$. With the Boussinesq approximation [i.e. $q(s,p) = 1$], G^* varies as $(q''x^4)^{1/5}$.

The transition parameter proposed here, $G_{BT}^* x^{1/5}$, can be nondimensionalized as $G_{BT}^*(gx^3/v^2)^{1/15}$ where (gx^3/v^2) represents a unit Grashof number. Velocity and thermal transition locations in this study are determined at the location where the maximum velocity and the surface temperature excess deviate from the laminar trend of increase. This criteria was used by Mahajan and Gebhart [18]. A value of $G_{BT}^*(gx^3/v^2)^{1/15}$ between 5500 and 5600 is found for the beginning of transition in all the experiments. The end of transition is not correlated because fully developed turbulence was achieved only in one or possibly two runs.

The measured velocity disturbance amplitude in both the laminar region and the transition are plotted in Fig. 8. The calculated relative disturbance velocity (u/u_{max}) distribution, from [21], is also shown. This profile has two peaks. The disturbance measurements near the inner peak are in good agreement with theory. Measurements also suggest another small peak near the outer edge of the boundary region. However, the agreement with the theory is poor. As discussed earlier, the effect of changing flow direction on the anemometry in this region is very large. This will cause a systematic deviation. As the flow undergoes transition, the measured disturbances spread in η, as also seen in Fig. 8.

In Fig. 9 the temperature disturbance data is compared with the calculated disturbance temperature profile. It was shown in [21] that such calculated profiles do not change their shapes over a wide range of G^*, from 90 to 550. However, the experimental data show a slight thickening of the disturbance profile with increasing G^*. The calculations [21] are based on small disturbances and linear stability analysis, and all these results cannot be extrapolated in very large G^* region. At low G^* values the data compares very well.

It is well known, see, for example [22], that as a disturbance is convected downstream, it is rather sharply filtered for a predominant component. This most amplified frequency is here called the characteris-

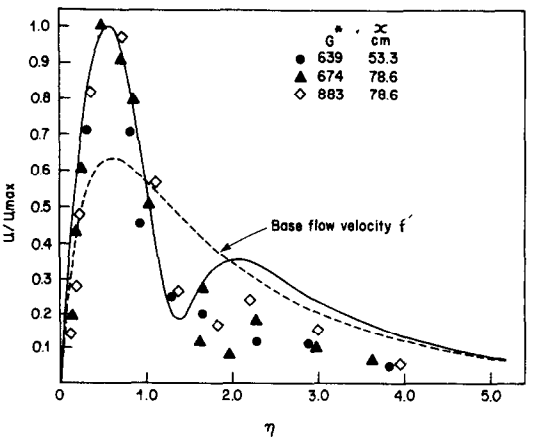

FIG. 8. Disturbance velocity distribution u/u_{max} across the boundary layer.

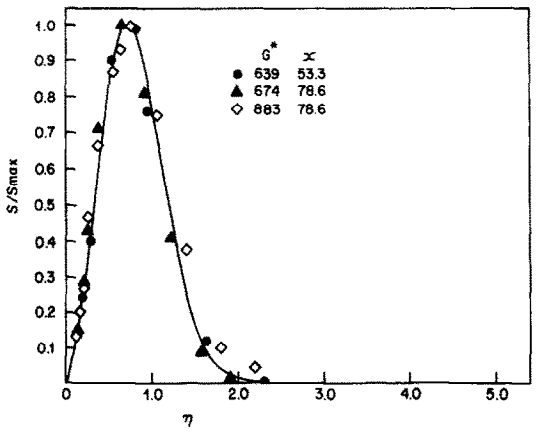

FIG. 9. Disturbance temperature distribution s/s_{max} across the boundary layer.

tic frequency, B^*. For a uniform flux surface it is related to the physical frequency and the surface heat flux as

$$\beta^* G^{*(q+1)/(q+3)} = \frac{2\pi f}{\nu}\left[\frac{g\alpha(s,p)}{\nu^2}\left(\frac{q''}{k}\right)^q\right]^{-2/(q+3)} = B^* \tag{5}$$

where $\beta^* = 2\pi f(4+q)^2 x^2/\nu G^{*3}$ and G^* is given in equation (4). It was shown by Qureshi and Gebhart [21] that for a uniform flux surface in cold water B^* is not single valued but increases slowly with G^*. In the G^* range of the stability plane in which measured frequencies were obtained here, $B^* = 1.343$ passes approximately through the minimum G^* of the amplification ratio contours. After performing the proper coordinate transformations the calculated [21] stability plane, amplitude ratio contours and a characteristic frequency path ($B^* = 1.343$) are shown in Fig. 10. These data points confirm that frequency filtering under the present ambient conditions is not as sharp as it has been found to be with an ambient at room temperature.

CONCLUSIONS

A buoyancy induced flow generated by a uniform flux surface in water at 4°C was studied experimentally. Surface temperature measurements were taken at 24 downstream locations for five different surface flux levels of 368, 634, 1389, 2414 and 3617 W/m^2. The transport rate in the laminar region is compared with the numerical calculations [12] and an excellent agreement is found. For the turbulent flow region, a heat transfer correlation is suggested, on the basis of somewhat limited data. The boundary layer was traversed with a hot film and thermocouple probe at five different downstream locations for various values of surface flux level. Boundary layer velocity and temperature measurements show good agreement with theory. Hot film calibration is given in detail. Temperature compensation for calibration is discussed.

A simultaneous velocity and thermal transition is found. Due to a weak buoyancy force, the transition is delayed and a new parameter is suggested to predict transition. Present results suggest the value of this parameter $G^*_{BT}(gx^3/\nu^2)^{1/15}$ between 5500 and 5600 for the beginning of transition. The disturbance velocity and temperature fields are determined and compared with the calculated profiles. Good agreement is found. The frequency filtering is not found to be very sharp, as also predicted by stability calculations.

Acknowledgements—The authors wish to acknowledge support for this study by the National Science Foundation under Grant ENG 77-21641.

REFERENCES

1. B. Gebhart and J. C. Mollendorf, A new density relation for pure and saline water, *Deep Sea Research* **24**, 831-848 (1977).
2. B. Gebhart and J. C. Mollendorf, Buoyancy-induced flows in water under conditions in which density extrema may arise, *J. Fluid Mech.* **89**, 673-707 (1978).

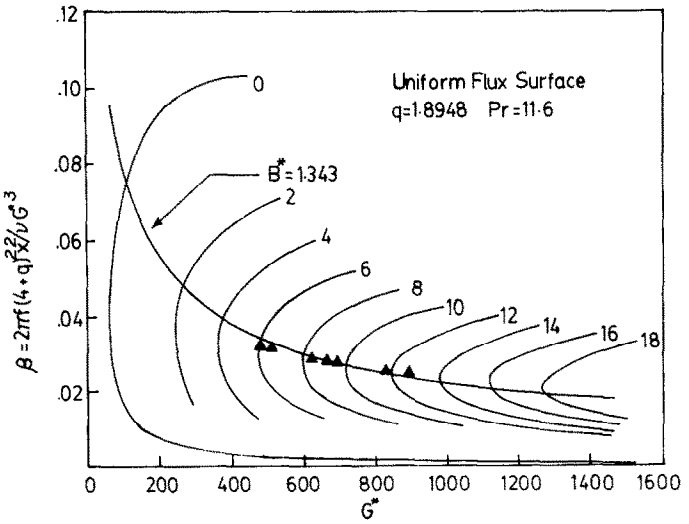

FIG. 10. Characteristic frequencies in transition observed experimentally. The stability plane is from [21] with transformed coordinates.

3. A. J. Ede, The influence of anomalous expansion on natural convection in water, *Appl. Sci. Res.* **5,** 458–460 (1955).
4. H. J. Merk, The influence of melting and anomalous expansion on the thermal convection in laminar boundary layers, *Appl. Sci. Res.* **4,** 435–452 (1953).
5. R. S. Schechter and H. S. Isbin, Natural-convection heat transfer in regions of maximum fluid density, *Am. Inst. chem. Engrs. J.* **4,** 81–89 (1958).
6. S. L. Goren, On free convection in water at 4°C, *Chem. Engng Sci.* **21,** 515–518 (1966).
7. C. R. Vanier and C. Tien, Further work on free convection in water at 4°C, *Chem. Engng Sci.* **22,** 1747–1751 (1967).
8. J. H. Perry, *Chemical Engineers' Handbook*, 4th edn, Section 3, p. 70 (1963).
9. C. R. Vanier and C. Tien, Effect of maximum density and melting on natural convection heat transfer from a vertical plate, *Chemical Engineering Progress Symposium Series* **64,** 240–254 (1968).
10. S. Roy, Free convection in liquids under maximum density conditions, *Ind. J. Phys.* **46,** 245–249 (1972).
11. Z. H. Qureshi and B. Gebhart, Vertical natural convection with a uniform flux condition in pure and saline water at the density extremum, *Proceedings of the 6th International Heat Transfer Conference*, Toronto, Vol. 2, pp. 217–222 (1978).
12. Z. H. Qureshi and B. Gebhart, A new formulation for buoyancy induced flow adjacent to a vertical uniform flux surface in cold water. *Num. Heat Transfer* **2,** 467–476 (1979).
13. Z. H. Qureshi and B. Gebhart, Transition and transport in a buoyancy driven flow in water adjacent to a vertical uniform flux surface, *Int. J. Heat Mass Transfer* **21,** 1467–1479 (1978).
14. H. Shaukatullah, Ph.D. Dissertation, Cornell University, Ithaca, New York (1977).
15. K. Hollasch and B. Gebhart, Calibration of constant-temperature hot-wire anemometers at low velocities in water with variable fluid temperature, *J. Heat Transfer* **94,** 17–22 (1972).
16. H. Shaukatullah and B. Gebhart, Hot film anemometer calibration and use in fluids at varying background temperature, *Lett. Heat Mass Transfer* **4,** 309–317 (1977).
17. H. Shaukatullah and B. Gebhart, Effect of flow direction on calibration of hot-film anemometers at low velocities, *J. Heat Transfer* **100,** 381–382 (1978).
18. R. L. Mahajan and B. Gebhart, An experimental determination of transition limits in a vertical natural convection flow adjacent to a surface (to be published) (1981).
19. F. Godaux and B. Gebhart, An experimental study of the transition of natural convection flow adjacent to a vertical surface, *Int. J. Heat Mass Transfer* **17,** 93–107 (1974).
20. Y. Jaluria and B. Gebhart, On transition mechanisms in vertical natural convection flow, *J. Fluid Mech.* **66,** 309–337 (1974).
21. Z. H. Qureshi and B. Gebhart, The stability of vertical buoyancy induced flows in cold pure and saline water (to be published) (1981).
22. B. Gebhart and R. L. Mahajan, Characteristic disturbance frequency in vertical natural convection flow, *Int. J. Heat Mass Transfer* **18,** 1143–1148 (1975).

MESURE DE TRANSPORT DE FLUIDE ET DE CHALEUR PAR UN ECOULEMENT NATUREL VERTICAL DANS L'EAU FROIDE

Résumé—On mesure des grandeurs de transport dans un écoulement vertical naturellement induit le long d'une surface à flux uniforme (1,3 m de haut), dans l'eau à 4°C. Les champs de vitesse et de température sont déterminés en des points différents pour plusieurs valeurs du flux entre 368 et 3617 W/m^2. On mesure les grandeurs moyennes et leurs perturbations et on compare avec la théorie. On trouve une transition simultanée dynamique et thermique. Du fait d'une dépendance non linéaire de la densité vis-à-vis de la température, la transition est retardée. Un nouveau paramètre est suggéré qui prédit le début de la transition. Le filtrage de fréquence dans les zones laminaire et de proche transition est trouvé peu aigu, comme prévu par la théorie. La fréquence calculée $B = 1{,}343$ est confirmée par l'expérience.

MESSUNGEN DES WÄRME- UND STOFFTRANSPORTS BEI VERTIKALEN, DURCH AUFTRIEB INDUZIERTEN STRÖMUNGEN IN KALTEM WASSER

Zusammenfassung—Es werden Messungen des Stofftransports in einer vertikalen, durch Auftrieb induzierten Strömung an einer Wand mit gleichförmiger Wärmestromdichte (Höhe 1,3 m) in Wasser von 4°C beschrieben. Geschwindigkeits- und Temperaturprofil werden an verschiedene Stellen stromabwärts bei mehreren Wärmestromdichten im Bereich von 368 bis 3617 W/m^2 bestimmt. Es werden sowohl die mittleren als auch die verteilten Größen gemessen und mit der Theorie verglichen. Es wurde ein gleichzeitiger Umschlag von Strömung und Wärmeübergang gefunden. Wegen einer nichtlinearen Dichteabhängigkeit von der Temperatur wird der Umschlag verzögert. Es wird ein neuer Parameter vorgeschlagen, der den Beginn des Umschlagvorgangs beschreibt. Die Frequenzfilterung im laminaren und zu Anfang des Übergangsbereichs hat sich als nicht sehr scharf herausgestellt, wie auch aufgrund von Rechnungen anzunehmen war. Die vorausberechnete Filterfrequenz $B^* = 1{,}343$ wurde durch die Experimente bestätigt.

ИЗМЕРЕНИЕ ТЕПЛО- И МАССОПЕРЕНОСА ПРИ СВОБОДНОКОНВЕКТИВНОМ ВОСХОДЯЩЕМ ТЕЧЕНИИ В ХОЛОДНОЙ ВОДЕ

Аннотация — Исследуется тепло- и массоперенос при восходящем свободноконвективном течении у равномерно нагреваемой поверхности высотой 1,3 м, помещенной в объем воды при температуре 4 С. Определяются поля скоростей и температур в нескольких точках у верхней части поверхности при изменении величины теплового потока в диапазоне от 368 до 3617 Вт/м^2. Измеряются значения средних и возмущенных величин и приводится сравнение с результатами теоретических расчетов. Показано возникновение одновременного динамического и теплового перехода, запаздывание которого происходит из-за нелинейной зависимости плотности от температуры. Для определения начала перехода предложен новый параметр. Найдено, что фильтрация частоты в области ламинарного и начале переходного режимов не имеет резких максимумов, что также подтверждается результатами расчетов. Расчетное значение частоты фильтрации $B^* = 1{,}343$ совпадает с измеренным.